Proceedings of the
Annual Stability Conference
Structural Stability Research Council
Charlotte, North Carolina, April 11-14, 2023

Experimental investigation on local stability enhancement of steel tubular profile introducing hybrid metal-polymer sections

Ieva Misiunaite[1], Arvydas Rimkus[2], Viktor Gribniak[3],

Abstract
During a year tubular sections successfully gained a leading positions in various structural applications. This type of the profile is approved by the architects and structural engineers. The first favor the aesthetics and integrity the shapes can provide, the second are attracted by the ease of manufacture, lightweight and structural features such as high resistance to torsional effects. Despite the years of design practice and application the strengthening under concentrated loads still raises structural challenges and highly increases the weight of the tubular sections. This study provides a new approach to increase the bearing capacity of the hollow sections under concentrated load by means of forming a hybrid metal-polymer section. The experimental program embeds slender rectangular steel hollow sections with adhesively bonded lightweight polymer infills. The additive manufacturing is utilized to create low density polymer stiffeners which increase the weight of the section only 28%. The tailored topology of the stiffeners prevents deformations of the flange whereas composite effect enhance resistance of the web to premature buckling. The polymer infill by itself increases the bearing capacity of the steel profile 35%, adhesive engagement enhance it to 85%. Local deformations caused the failure of the reference specimens without reinforcement. On the contrary, the failure of the hybrid metal-polymer section grounds the possibility to increase the bearing capacity and deformation energy absorption of the slender sections by preventing premature buckling of the web as well as reinforcing the flange and ensuring efficient use of materials.

1. Introduction

During a year tubular sections successfully gained a leading positions in various structural applications. This type of the profile is approved by the architects and structural engineers. The first favour the aesthetics and integrity the shapes can provide, the second are attracted by the ease of manufacture, lightweight and structural features such as high resistance to torsional effects.

The manufacturing of steel sections simply may be divided in two premier methods known as hot rolling and cold forming. The choice of cold formed steel over the hot rolled products is

[1] Senior Researcher, Vilnius Gediminas Technical University, <ieva.misiunaite@vilniustech.lt>
[2] Senior Researcher, Vilnius Gediminas Technical University, <arvydas.rimkus@vilniustech.lt>
[3] Professor, Vilnius Gediminas Technical University, <viktor.gribniak@vilniustech.lt>

based on the ease of fabrication, versatility in application and high strength to weight ratio. These advantages of cold formed steel result into reduced material cost as well as labour required to assembly the structure (AISI Revision 2006). The use of thin sheets in cold forming determines the geometry of the sections to be slender and contributes to the element strength. Thin web and flange elements comprising a cold formed section have an inherent sensitivity to local buckling when subjected to compressive loads. On one hand, individual parts (webs and flanges) of cold formed steel sections can be idealized as rectangular thin plates simply supported along the edges and subjected to locally distributed in-plane edge compressive forces (Zhou, Young 2006, AISI S100 2016). On the other hand, the behaviour of webs and flanges within the cross section is interactive.

The elastic buckling of individual flat rectangular plates under locally distributed edge forces has been studied by numerous researchers (Yu *et al.* 2019). The critical elastic buckling load can be computed using theoretical formulae which is provided in many international design codes. However, the interaction between web and flange results in some kind of stiffened compression elements which will not collapse when the elastic buckling load is reached but will develop post-buckling strength by means of redistribution of stresses (Zhou, Young 2006) and leads to inelastic buckling behaviour.

When the localized failure of structural section is caused by the concentrated load or reaction applied on the short element previously mention buckling failures as well as web yielding might be distinguished and are known under common name of web crippling. In cold formed steel sections design, web crippling is among the most critical failure mechanisms to be considered. Local yielding of the web at the web and flange junction, flange crushing followed by web buckling and, or a combination of the aforementioned failure modes are the mechanisms through which a member subjected to web crippling may fail.

1.1 *Strengthening of cold formed sections*

Web crippling is one of the most important failure modes that must be considered in the design of cold formed steel members. This is because it is not easy to strengthen steel tubular sections.
The stiffening of steel hollow sections started with the external strengthening and went through many different stages following the development of the materials and joining methods. It started with adding the reinforcing steel plates which were either welded or bolted to the main profile and led to application of fibre reinforced polymer (FRP) joined with adhesive bonding technique. Strengthening using additional steel plates is associated with many drawbacks. Adding a considerable weight to strengthened elements and fatigue problems associated with welding process are samples of these obstacles (Abu-Sena *et al.* 2019). Several studies have shown that either CFRP plates or wraps can be used to effectively strengthen steel tubular sections (Abu-Sena *et al.* 2019, Fernando *et al.* 2009, Zhao *et al.* 2006). A reasoned review on research works covering the efficiency of FRP strengthening systems on metallic structures was presented by Zhao (2017). This review concluded that; the strengthening performance using FRP mainly depends on the bond between FRP and strengthened steel elements.
There were also attempts to increase web crippling capacity of tubular sections by internal strengthening. The first attempts employed partial filling with wood or concrete (Zhao 1999). The latest internal strengthening methods as well as external emphasis FRP strengthening systems. The extensive study of Zhao *et al.* (2006) on CFRP strengthened rectangular hollow

sections reviled that the applied methods significantly increased the web crippling capacity especially for those sections with large web depth-to-thickness ratio and internal CFRP plates.

Alternatively, the deformational behaviour of thin-walled structures might be increased using cellular filler materials. Metallic composite systems embedding polymeric and metallic foams as well as honeycombs enable to absorb energy under mechanical loading (Duarte *et al.* 2014). Among different techniques applied producing the core material, additive manufacturing (3D printing) has been frequently considered due to the prominent advantages of mass customisation and the ability to create complex structures (Ngo *et al.* 2018, Kumar, Sathiya 2021). The performed studies have shown the potential of the 3D printing for customising and optimising core element topologies avoiding constraints resulting from conventional manufacturing techniques. Additive manufacturing offers the ability to develop resilient composite structures tailored accordingly to operational applications.

1.2 *Developing a hybrid section*

The previous study of Gribniak *et al*. (2022) demonstrated the efficiency in improving the local stability of metallic section introducing the hybrid system comprising aluminium profile and low modulus internal polymeric stiffeners. The performed study considered aluminium section with explicitly expressed elastic local buckling. Although the main efficiency of the considered element under compression load was determined by the adhesive bonding the polymer stiffener contributed in altering the buckling mode of the aluminium section and increasing buckling capacity. This study aims to continue previous work, generalize the proposed system and translate the idea to conventional cold-formed steel rectangular hollow sections (RHS).

A cold formed steel rectangular hollow section with slender webs available on the market is the subject of the study. The previous investigation (Gribniak *et al*. 2022) has determined the research object choice for producing the composite cross-section with polymer infill, expecting the polymer stiffeners' effect on the buckling behaviour of the webs. When considering section as array of adjacent plate elements not only the slenderness but also the boundary conditions play the role in determining buckling behaviour of the integrate parts. It is commonly assumed that the web and flange within the section are prevented from the translational deformations and the restraints are dependent on the rotational stiffness. The rotational stiffness by means of flexural deformations of the flange might be increased by the use of intermediate stiffeners. Moreover, the technological requirements for forming tubular steel sections by bending thin sheets result in rounded corners between web and flange. The external corner radius introduces load eccentricity and additional bending moment in the webs, which increases web flexural behaviour and reduces web buckling capacity. It is expected that the polymer stiffener will provide a sufficient support for the flange decreasing its deformations and increasing rotational stiffness as well as decreasing the eccentricity of the compression load translated to the web.

A low deformation modulus thermoplastic polymeric material was used to produce the inner stiffeners. A 3D printing technology was utilized to tailor the geometry of the infill. Shkundalova *et al*. (2018) investigated the mechanical properties and tensile failure of thermoplastic polymeric materials including acrylonitrile butadiene styrene (ABS), polylactic acid (PLA), high impact polystyrene (HIPS), and polyethylene terephthalate (PETG). The study revealed that the ultimate strain of the samples made of ABS, HIPS and PETG localised between the printed

filaments resulting in local brittle failure of the tensile specimens. On the contrary, the PLA featured a ductile failure providing the highest nominal tensile strength (42.06 MPa) among the considered polymers and elasticity modulus of 100% density material E = 2.2 GPa. Thus, the 3D printing in this study employs PLA.

This study introduces the hybrid metallic-plastic system comprising conventional steel section and low deformational modulus thermoplastic infill to increase the load-bearing capacity of slender RHS. The experimental program embeds a short segment of slender rectangular steel hollow sections with adhesively bonded lightweight polymer infills. The additive manufacturing is utilized to create low density polymer stiffeners which increase the weight of the section only 28%. The study aims to present the effect of the integrate parts of the proposed system (polymer infill and adhesive bonding) on the buckling behavior of webs of considered steel section.

2. Test Specimens

The tests were carried out in the Laboratory of Innovative Building Structures at VILNIUS TECH. The test subject was a rectangular hollow section profile made from the S355 grade steel available on the market. The stiffeners were produced using a 3D printing technique. They had cross -sectional dimensions reflecting the internal shape of the RHS (Fig. 1d) and 15 mm length; thus, 6 segments, stuck together with epoxy adhesive, strengthened each profile.

The stiffeners were printed using a PRUSA i3 MK3 printer with identical printing parameters: extrusion nozzle temperature = 215°C; printing bed temperature = 60° C; print speed = 28 mm/s. The 1.75 mm PLA filament *Prusament* having 1240 kg/m^3 density was used. The stiffeners were printed in the horizontal position; the thickness of each printing layer was 0.5 mm. Two continuous "shells" having 100% density were printed on the perimeter of each specimen. The inner part of the samples was produced at rectilinear raster orientation inclined at 45°. Such printing layout is frequently used for prototyping.

Four specimens were produced to investigate local deformations and failure mechanism of the hybrid section fragments under compression. The length of the samples was equal to 100 mm; the steel segments utilized from 200 mm depth and 100 mm width steel profile with the 4 mm wall thickness (Fig. 1b). Two types of composite samples were produced to investigate the effect of individual components (polymer stiffener and adhesive bonding) on the overall behaviour of the developed hybrid section. One of them comprised steel section and polymeric stiffener without the adhesive fixation (Fig. 2c); another was adhesively bonded hybrid section. Six 15 mm thickness stiffeners were inserted in the centre part of the steel segment. Two items of each type were produced. It should be noted that the plastic stiffeners resemble the idealized geometry of the inner steel profile without consideration of initial geometric imperfections. Initially deformed shape of the steel profile (Fig. 1c) caused technical difficulties for adhesive bonding and resulted in rough and imperfect contact (Fig. 1f).

Besides composite specimens, two additional samples of bare plastic stiffener (Fig. 1e) and steel hollow section (Fig. 1a) were delivered as references to investigate strength enhancement in composite section. The stiffeners used for the investigation had a 25% infill density.

Fig. 1 shows all of the compression specimens. For all of the specimens the monitoring surfaces were spray painted to apply a high-contrast random pattern. Additional to linear variable displacement transducers (LVDT) used for displacements monitoring the linear deformations of specimens were monitored using a digital image correlation (DIC) technique.

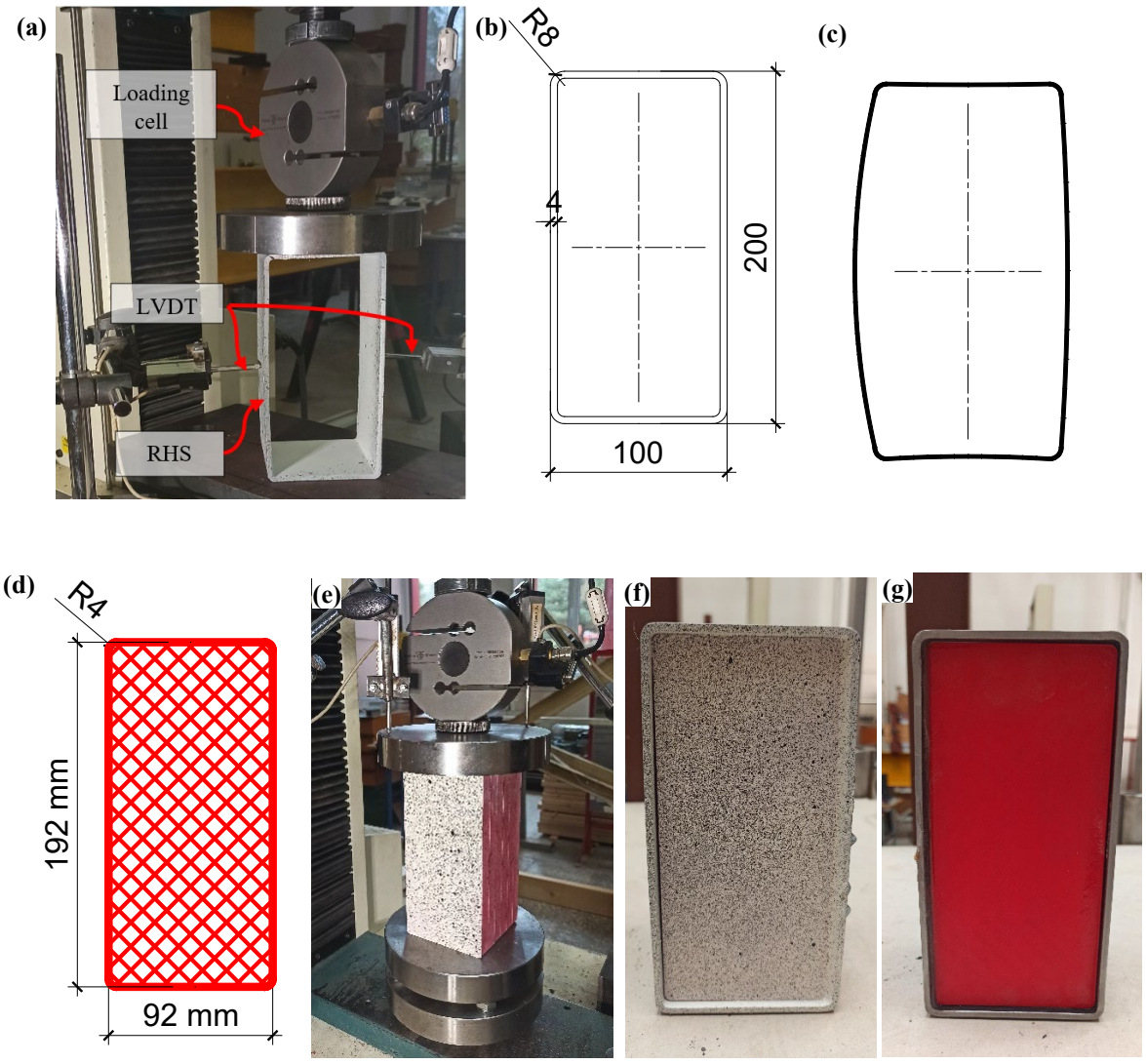

Figure 1. Compression specimens: (a) test set-up of reference steel rectangular hollow section (RHS), (b) Cross-section dimension of RHS, (c) shape of initial imperfections in steel profile, (d) dimensions and inner topology of polymer stiffener, (e) test-set up of bare polymer infill, (f) and (g) composite section with and without adhesive fixation, respectively

Ten tensile coupons were also tested to determine the mechanical properties of the steel: four specimens were cut from flange and eight from web (Fig. 2b). The test samples were designated correspondingly as F-1 – F-4 and W-1 – W-6 excluding two samples which failed outside the measuring zone.

3. Measurement results

3.1 Tensile tests

The tests were carried out using a 200 kN tensile machine *P-20* with a loading rate of 100 N/s. Figure 2 illustrates the tensile tests. The extensometer *MFA 25-12* (Fig. 2a) measured deformations of the test samples. The gauge length of the tensile coupons was equal to 50 mm. The geometry of the tensile coupons corresponds to the standard EN ISO 6892-1 (2016) requirements.

A failure outside the measuring zone caused the loss of the experimental data of two sample extracted from the web. Figure 3 shows the stress-strain diagrams estimated from the tensile tests. Table 1 lists the determined mechanical parameters of the steel samples, including elastic modulus (E), yield strength (f_y), ultimate tensile strength (f_u), and ultimate strain (ε_u).

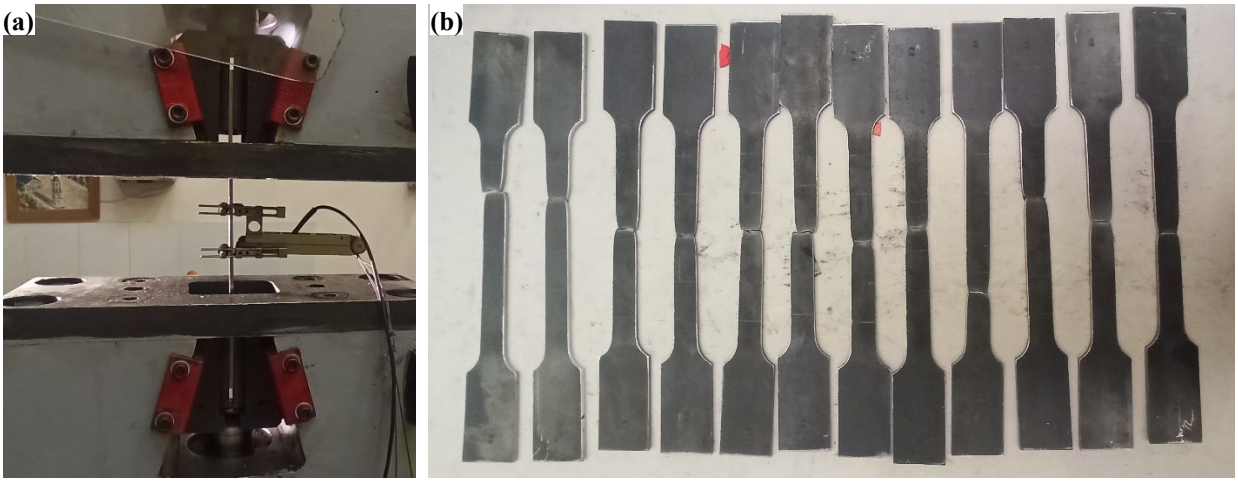

Figure 2. Tensile tests: (a) coupon equipped with an extensometer; (b) sample after testing

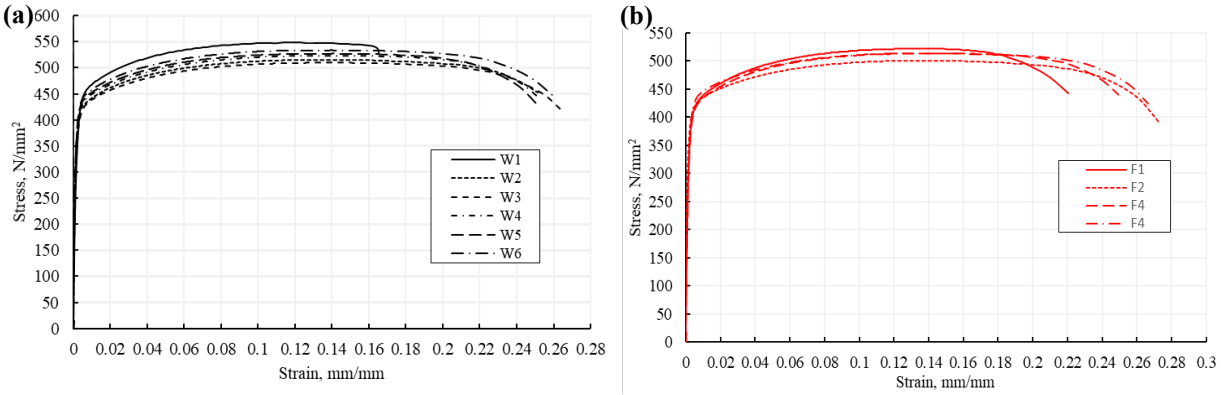

Figure 2. Stress-strain diagrams of stell: (a) specimens W-1-W6; (b) specimens F-1-F4

Table 1. Steel tensile coupons test results

Assembly no.	Coupon test ID	Elastic modulus E (N/mm^2)		Yield Strength f_y (N/mm^2)		Ultimate Strength f_u (N/mm^2)		Ultimate Strain ε_u (mm/mm)	
			AVR.		AVR.		AVR.		AVR.
A1	W1	266026	228122	426	411	549	527	0.1198	0.1433
	W2	252507		429		516		0.1503	
	W3	242078		412		511		0.1500	
	W4	206720		351		523		0.1594	
	W5	175841		422		529		0.1405	
	W6	225559		429		534		0.1399	
A2	F1	187345	189217	412	410	522	512	0.1420	0.1544
	F2	171737		412		501		0.1588	
	F3	190434		400		514		0.1563	
	F4	207354		415		513		0.1604	

2.2 Compression tests

The compression tests of bare steel and polymer stiffener samples were carried out using a 75 kN electromechanical machine *H75KS* (*Tinius Olsen*, Norway) under displacement control (loading rate = 1 mm/min). Linear variable displacement transducers (LVDT) with 0.001 mm precision measured the horizontal displacements of the RHS webs and vertical displacements of the polymer infill; a 75 kN load-cell monitored the applied load. The specimens were tested until the failure. Figs. 1a and 1e shows the test setup. For the compression test of composite sections a 100 kN electromechanical machine under displacement control was utilized. The loading rate was applied in the same manner as for the reference steel and polymer samples (1mm/min) and LVDT were used to measure vertical displacements of the test specimens.

Additionally, deformations of the specimens were monitored using a digital image correlation (DIC) technique. The spray paint was utilised to apply a high-contrast random pattern to the monitoring surface (Figs. 1a, e and f). The digital images were captured by a digital single-lens reflex camera *Canon EOS 77D SLR* with 18-135 mm *Canon EF-S* lens placed on a tripod at 0.4 m from the monitored surface. The 6000×4000 pixel images were captured at the load increments of 1 kN using the following settings of the camera: exposure time = 1/200 s, aperture = f/4.5, sensitivity to light = ISO 100, focal length = 24 mm. A remote control device was used to avoid unexpected movements of the camera.

Figure 3 shows the characteristic failures of all compression specimens—the inelastic buckling is characteristic failure of the reference steel specimens (Fig. 3a); the crushing of the vertical surfaces indicates the failure of the polymer stiffener (Fig. 3b); delamination of the webs of the steel profile indicates the loss of adhesive fixation (3c); the combination of aforementioned failures characterise the final failure of composite section (Fig. 3d). This finding corresponds to the experimental results reported in the previous study (Gribniak *et al*. 2022), demonstrating similar failure mechanism of the composite section.

The differences of the failure modes of the strengthened specimens with and without adhesive fixation after the compression tests are not evident and both resemble the failure presented in Fig. 1d. The load-displacement diagrams, shown in Figure 4, are more informative in this

context. The stiffeners' adhesive connection increases the ultimate load more than four times, altering the deformation response of the compression specimens.

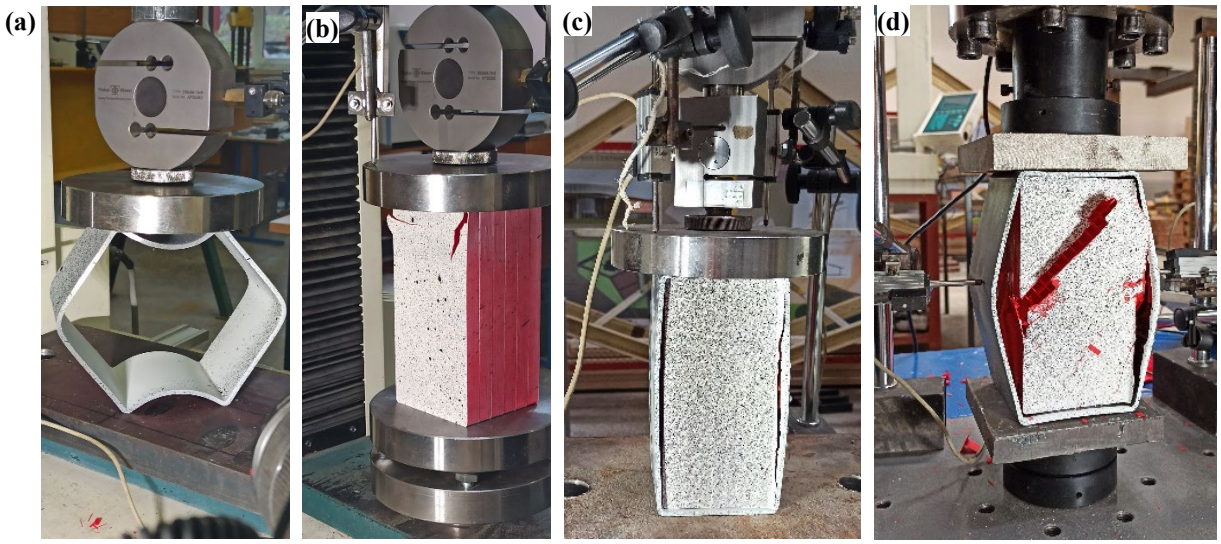

Figure 3. Compression tests: (a) test apparatus; (b) strengthened sample; (c) a typical failure; (d) a failure of the composite section

Figure 4 presents the load-displacement diagrams depicting ultimate load of each test specimen and summarises the results of the compressive tests. The blue curves referring to the deformational behaviour of the composite section without adhesive fixation demonstrate that the polymer infill governs the stiffness of the composite profile. The scatter of the ultimate load is associate to the size of the initial imperfections in steel section. The average compression load corresponding to the loss of the steel strength is equal to 66.2 kN; the values 65.0 kN and 69.3 kN define the variation interval of the corresponding load. The black curve depicts the effect of the adhesive fixation. Fig. 4 shows that the adhesive bonding of the inserted polymer has a substantial effect on the strength of the section. The points "1" and "2" refer to the delamination of the steel profile webs. The asynchronous delamination of the webs is associate to the asymmetry of the initial deformed shape of the steel profile (Fig. 1c) and irregular adhesive bonding connection.

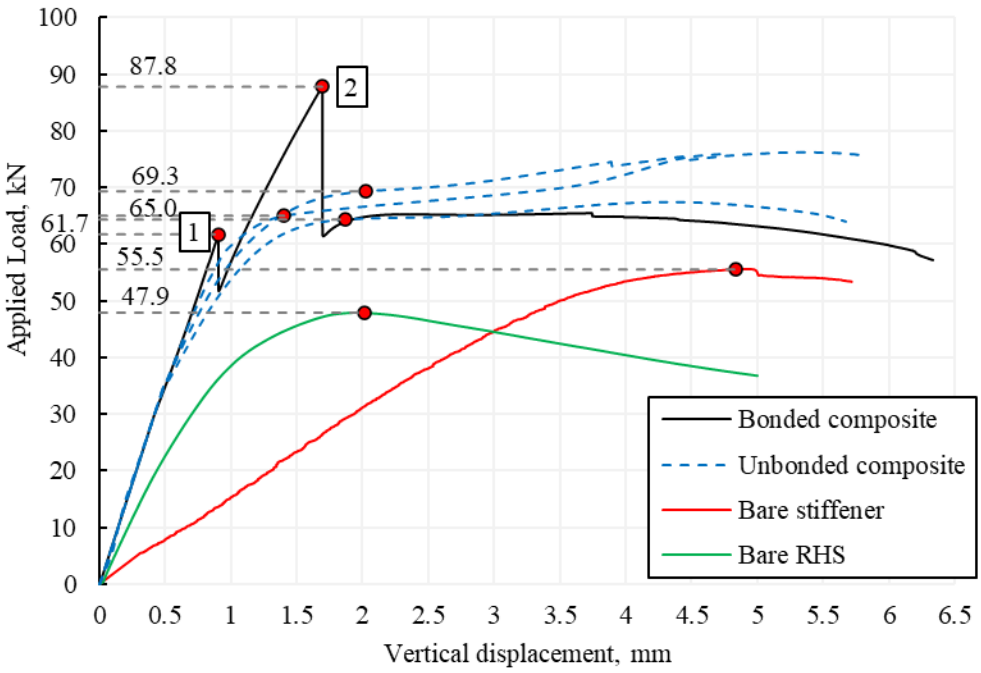

Figure 4. Load-vertical displacement diagrams of the compression specimens

3. Numerical analysis

The numerical analysis provides a comparison between failure mechanism of bare steel profile and composite section as well as gives a definitive explanation of the effect of polymer stiffeners on the buckling behaviour of the steel profile webs. The geometrical and material nonlinear analysis was performed using the commercially available software ABAQUS (2011).

Three individual finite element (FE) models were created to reflect the behaviour of the bare RHS, bare stiffener and composite section without adhesive fixation. The FE models were built using the commercially available software package ABAQUS (2011). All three models comprised considered steel section, bearing and loading plates as shown in Fig 5. The general purpose linear 4-sided shell element S4R with reduced integration was used to model the steel section and polymer stiffener. The baring plate (Fig. 5) was modelled as a fixed discrete rigid body. The boundary conditions (BC) were applied through the reference point. The ‘‘surface to surface contact’’ option provided in ABAQUS was employed for the interaction between the bearing plate and the steel section.

The loading plate (Fig. 5) was modelled as a fixed discrete rigid body except for the vertical displacement. The contact between loading plate and steel profile was described in the same manner as for the base plate and steel tube. The displacement controlled load was applied introducing the vertical displacement at the reference point of the loading plate.

The average measured material properties provided in Table 1 were used to describe material behaviour of steel RHS. The different mechanical properties were applied for the web and flange corresponding to the average values computed after tensile coupon test. The Poisson’s ratio was

taken as nominal value of 0.3. The elastic – plastic material model with strain hardening was employed to reflect the behaviour of the steel. The effect of geometrical imperfections was considered through the elastic buckling analysis. To introduced the initial deformed shape the interaction of the local and global buckling modes was considered with the amplitude equal to the manufacturing tolerances prescribed in the design standards (CEN 2008). The effect of the residual stresses was found to be negligible and was thus ignored in the model.

The set of 6 individual plastic stiffeners featuring the inner shape of the steel RHS and the length of 15 mm was modelled to reflect the experimental sample of bare stiffener as well as plastic part of the composite section (Fig. 5). The interaction between adjacent individual stiffeners within the set was described as tied referring to the adhesive bonding used for the experimental samples. The material of polymer stiffeners was simplified to isotropic and described as elastic-perfectly plastic utilizing the tensile modulus and yielding stress described in Section 1.2.

The contact between polymer stiffener and the bearing and loading plates was described using ‘‘surface to surface contact’’. For the normal behaviour the “hard contact” option with Augmented Lagrange multiplier and reduced stiffness scale factor to 0.01 was found the best option to enforce the contact constraints. The penalty enforcement method with friction coefficient of 0.3 was applied to define interaction in the tangential direction. The contact between steel profile and polymer infill was described as “soft”. For the normal behaviour the “hard contact” option with linear penalty enforcement method and reduced stiffness scale factor to 0.01 was found the best option to model the contact between two deformable bodies to avoid over constraint. The penalty enforcement method with friction coefficient of 0.3 was applied to define interaction in the tangential direction.

A mesh sensitivity study was conducted resulting in an appropriate mesh for the numerical modelling presented in this paper. For the steel profile rather coarse mesh of 10 mm FE size was used as it provided a good agreement between experimental and numerical results and highly reduced the required computational time. The mesh used for the plastic stiffener was varying in size with the largest element size of 4 mm in the less geometrically complex parts and the smallest element size at the corner regions as well as the intersection of vertical and contour surfaces (Fig. 5).

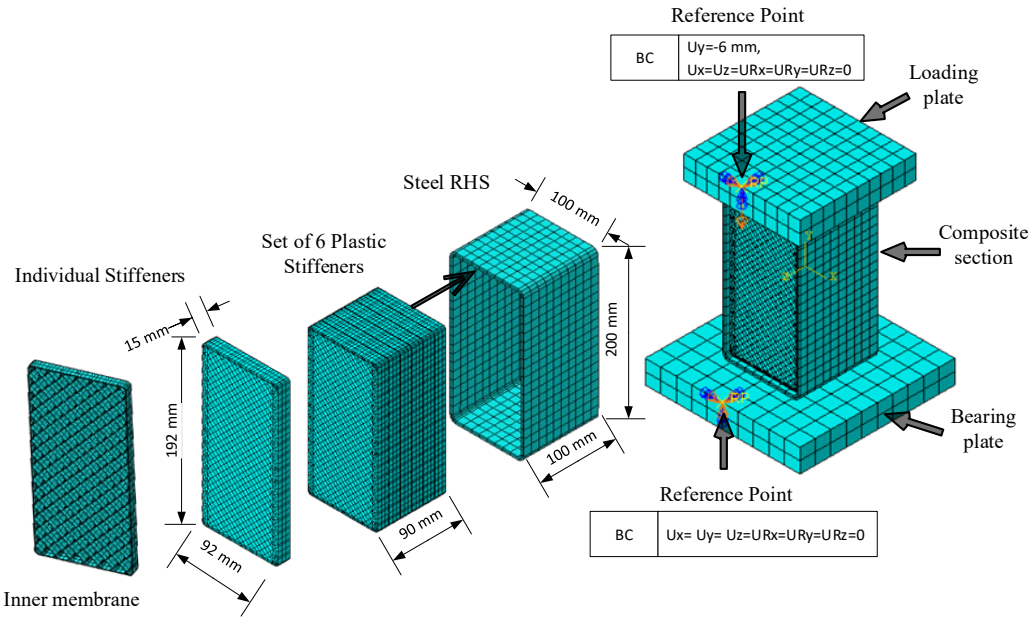

Figure 5. FE modelling (Ux, Uy, Uz – correspond to the translational degree of freedom and URx, URy, URz – rotational degree of freedom)

4. Results and discussion

Figure 6 shows the comparison between computational and experimental load-vertical displacement relationships of bare polymer stiffener. Considering complex geometry of the stiffener and simplified isotropic elastic-perfectly plastic material model FE model provided quate accurate results. The model enabled accurately capture the point of yielding initiation (point A in Fig. 6) and the difference between experimental and computational peak load (point B in Fig. 6) was just 1%. Slightly higher errors can be observed comparing elastic part of the curves although the highest error didn't exceed 8%.

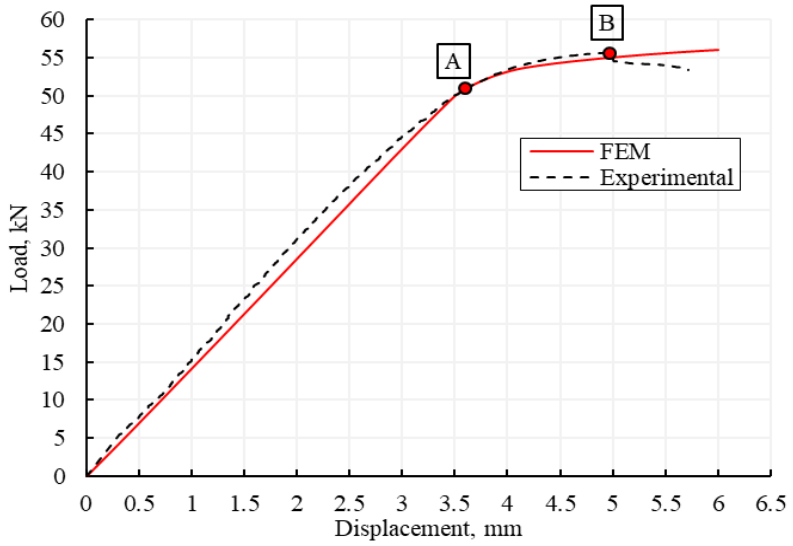

Figure 6. Validation of bare stiffener FE model: Load-vertical displacement relationship

The predicted load-web displacement curves for bare RHS are compared with the experimental results in Fig. 7. The FE provided very accurate predictions for the peak load with negligible underestimation. Comparing "Web #1" and "Web #2" deformations a slightly smaller deformation of the "Web #2" can be observed in the Fig. 7. The difference in the web deformations is the result of initial imperfections which in the case of interactive global and local imperfections determines an asymmetric initial deformed shape of the section (Shen, Wadee 2019). The "Web #1" FE predicted deformation behaviour of the web closely match experimental results though the "Web #2" predictions show some inaccuracy. This inaccuracy might be initiated by the modeling simplification of initial imperfections. As mentioned in the Section 3, initial geometrical imperfections were considered utilizing linear local and global buckling modes and scaling the amplitude to the corresponding nominal values of manufacturing tolerances provided in the standards. In case of "Web #2" the nominal value for out of flatness could be assumed higher than actual one and resulted in higher computational deformations than measured experimentally.

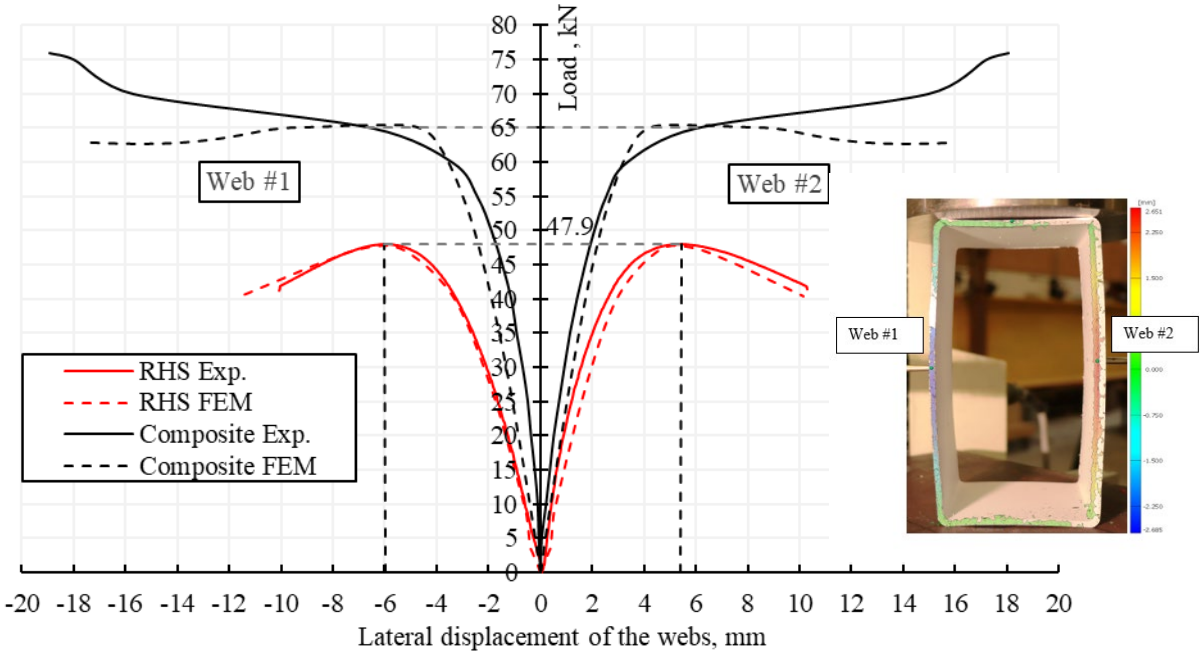

Figure 7. Validation of FE model: Load-web displacement relationship

Figure 7 also presents the comparison between computational and experimental load-web displacement relationships of composite section without adhesive fixation. Considering complex contact behavior between steel profile and polymer stiffener the numerical analysis provides adequate predictions for the elastic behavior (the maximum error do not exceed 26%) of the composite section as well as average compression load of 65.0 kN as shown in Fig. 4. On one hand, due soft contact conditions between steel section and plastic stiffener the FE simulation was not able to replicate the stiffening part of the experimental curves. On the other hand, in case of hard contact conditions the numerical analysis resulted in over constraint and provided inadequate solution. Assuming the corresponding load as the bearing strength of the composite section the computational model was considered as satisfactory and relevant for further analysis.

The comparative analysis of the results presented in Fig. 7 explains the polymer stiffener contribution to the buckling behaviour of the webs of the steel RHS. The polymer stiffener provides the sufficient support for the steel profile flange and increases the rotational stiffness at the web and flange junction. This observation is supported by the increased web stiffness and decreased deformations of the composite section as shown in Fig. 7. Moreover, the difference in ultimate loads of bare RHS and composite section without adhesive fixation depicted in Figs. 4 and 7 shows the 35 % strength enhancement. However, the contribution of plastic stiffeners by themselves in the load increase from 41.9 kN to 65.0 kN (Fig. 4), is insignificant and cannot indicate the composite section load-bearing capacity increase. At the same time, the adhesion effect corresponding to "black" curve in Fig. 4 substantially increases the load-bearing resistance of the considered composite element. The web adhesion nearly double the hybrid cross-section load-bearing capacity (compare 41.9 kN and 87.8 kN values in Fig. 4). Thus, developing a reliable adhesive connection between the steel profile and stiffeners should be the object of the further research.

5. Conclusions

This study demonstrates the efficiency of the hybrid system comprising steel profile and adhesively bonded low-modulus polymer stiffeners. The polymer stiffeners produced using a 3D printing technique strengthened samples for compression tests. Furthermore, the numerical analysis provides a definitive explanation of the polymer stiffener's contribution in the proposed hybrid system. The following conclusions are formulated from the obtained results:

- The application of the low-modulus polymer stiffeners, (with the elasticity modulus of ≈ 0.22 GPa) provides sufficient support for the flange of the steel section increasing rotational stiffness and results in increased buckling capacity of the webs.
- The compression tests demonstrated that the application of the adhesively fixed low-modulus stiffeners increases the ultimate load nearly two times. The adhesive bonding of the inserted polymer has a substantial effect on the web deformational behaviour preventing them from premature buckling. Despite the rough contact between the stiffener and steel profile caused by the initial imperfections of steel section, the compression load corresponding to the loss of the adhesive bond was equal to 87.8 kN. After debonding of the webs the load dropped to 65.0 kN corresponding to the bearing capacity of unbonded composite section.
- The satisfactory results of the numerical analysis comprising composite section (the peak load prediction error does not exceed 8%) allow employing this computational model to develop efficient hybrid systems including steel profiles with slender webs and low-modulus internal stiffeners.
- The results of the tests and numerical simulations allow relating the stiffeners' adhesion effect to the significant increase in the load-bearing capacity of the steel profile samples. Thus, developing a reliable adhesive connection between the steel profile and polymeric stiffeners should be the object of further research.

Acknowledgments

The authors acknowledged financial support received from European Regional Development Fund (Project No 01.2.2-LMT-K-718-03-0010) under grant agreement with the Research Council of Lithuania.

References

ABAQUS. (2011). “Analysis User's Manual, Version 6.11”. ABAQUS Inc.

Abu-Sena, A. B., Said, M., Zaki, M. A., Dokmak, M. (2019). “Behaviour of hollow steel sections strengthened with FRP”. *Construction and Building Materials*, 205 306-320.

AISI S100. (2016). “North American Specification for the Design of Cold-formed steel Structural Members”. *North American Cold-formed Steel Specification*. American Iron and Steel Institute: Washington, D.C.

AISI. (Revision 2006). “Web Crippling Data and Calibrations of Cold Formed Members”. *Research report RP00-2*, *October 2000*. American Iron and Steel Institute: Washington, D.C.

CEN. (2008). Execution of steel structures and aluminium structures - Part 2: Technical requirements for steel structures. Brussels, Belgium: CEN.

Duarte, I., Vesenjak, M., Krstulović-Opara, L. (2014). “Dynamic and quasi-static bending behaviour of thin-walled aluminium tubes filled with aluminium foam.” *Composite Structures,* 109 48-56. https://doi.org/10.1016/j.compstruct.2013.10.040

Fernando, D., Yu, T., Teng, J. G., Zhao, X. L. (2009). “CFRP strengthening of rectengular steel tubes subjected to end bearing loads: Effect of adhesive properties and finite element modelling.” *Thin-Walled Structures*, 47, 1020-1028. doi:https:// doi:10.1016/j.tws.2008.10.008

Gribniak, V., Rimkus, A., Misiunaite, I., Zakaras, T. (2022). “Improving local stability of aluminium profile with low-modulus stiffeners: Experimental and numerical web buckling analysis.” Thin-walled Structures, 172(108858). doi:https://doi.org/10.1016/j.tws.2021.108858

International Organization for Standardization (ISO). (2016). “Metallic material – Tensile testing – Part 1: Method of test at room temperature EN ISO 6892-1: 2016”. ISO, 2016.

Kumar, M.B., Sathiya, P. (2021). “Methods and materials for additive manufacturing: A critical review on advancements and challenges.” *Thin-Walled Structures*, 159 107228. https://doi.org/10.1016/j.tws.2020.107228.

Ngo, T.D., Kashani, A., Imbalzano, G., Nguyen, K.T., Hui, D. (2018). “Additive manufacturing (3D printing): A review of materials, methods, applications and challenges.” *Composites Part B: Engineering*, 143 172–196. https://doi.org/10.1016/j.compositesb.2018.02.012.

Shen, J., Wadee, M. A. (2019). “Local-global mode interaction in thin-walled inelastic rectangular hollow section struts part 1: Nonlinear finite element analysis.” *Thin-Walled Structures*, 145, 106183. doi:https://doi.org/10.1016/j.tws.2019.106183

Shkundalova, O., Rimkus, A., Gribniak, V. (2018). “Structural application of 3D printing technologies: mechanical properties of printed polymeric materials.” *Science–Future of Lithuania*, 10. doi:https://doi.org/10.3846/mla.2018.6250

Yu, W. W., LaBoube, R. A., Chen, H. (2019). “Cold-Formed Steel Design (5th Edition ed.).” John Wiley and Sons Inc., New York.

Zhao, X. L. (1999). “Partially stiffened RHS sections under transverse bering force.” *Thin-Walled Structures*, 35, 193-204. doi:https://doi.org/10.1016/S0263-8231(99)00023-3

Zhao, X. L. (2017). “FRP-Strengthened Metallic Structures (1st ed.).” CRC Press, Taylor & Francis Group, Boca Raton.

Zhao, X. L., Fernando, D., Al-Mahaidi, R. (2006). “CFRP strengthened RHS subjected to transverse end bearing force.” *Engineering Structures*, 28, 1555-1565. doi: https://doi.org/10.1016/j.engstruct.2006.02.008.

Zhao, X. L., Zhang, L. (2007). “State-of-the-art review on FRP strengthened steel structures.” *Engineering Structures*, 29, 1808-1823. doi:https:// doi:10.1016/j.engstruct.2006.10.006.

Zhou, F., & Young, B. (2006). “Yield line mechanism analysis on web crippling of cold-formed stainless steel tubular sections under two-flange loading.” *Engineering Structures*, 880-892. doi:https:// doi:10.1016/j.engstruct.2005.10.021.